Enhancing fouling resistance of polyethylene anion exchange membranes using carbon nanotubes and iron oxide nanoparticles

Carolina Fernandez-Gonzalez[a, b,*], Bopeng Zhang[b], Antonio Dominguez-Ramos [a], Raquel Ibañez[a], Angel Irabien[a], Yongsheng Chen[b]

[a] Departamento de Ingenierías Química y Biomolecular, ETS Ingenieros Industriales y de Telecomunicación, Universidad de Cantabria, Avda. Los Castros, s.n., Santander, 39005, Spain

[b] School of Civil and Environmental Engineering, Georgia Institute of Technology, Atlanta, Georgia, 30332, USA

*Corresponding author: fernandezgoc@unican.es, telephone: +34942206778

Abstract

This work presents the enhancement of organic fouling resistance of nanocomposite anion exchange membranes made from a commercial polyethylene anion exchange membrane and a negative thin layer. This layer is composed of sulfonated poly (2,6-dimethyl-1,4-phenylene oxide) (sPPO) and two nanomaterials of different geometry and composition, oxidized multi-walled carbon nanotubes CNTs-COO^- (0.2% $g \cdot g^{-1}$ to 0.8% $g \cdot g^{-1}$) or sulfonated iron oxide nanoparticles Fe_2O_3-SO_4^{2-} (0.2% $g \cdot g^{-1}$ to 0.6% $g \cdot g^{-1}$). The novel nanocomposite membranes showed a relevant improvement in fouling resistance caused by the modification of some physicochemical characteristics of membrane surface such as charge, roughness and hydrophilicity. The nanocomposite layer did not show a change in the membrane resistance. No remarkable differences were detected when changing the nanomaterial during characterization of nanocomposite membranes. The optimized loading of iron oxide nanoparticles and carbon nanotubes at 0.4% and 0.6% improved membrane fouling resistance by 45% and 53%, respectively. The improved fouling resistance of the best nanocomposite membranes AM-0.6CNTs remained after 12 hours of operation. Energy savings between 49% and 60% were also achieved.

1. Introduction

Desalination is becoming essential for maintaining a supply of fresh water in countries under water shortages. Electrodialysis (ED) is a technology used in fresh water production from different sources, sharing 3.6% of the total desalination capacity in 2014 with an installed capacity of 2.5 million $m^3 \cdot day^{-1}$[1]. In ED, ionic components are selectively transported through ion exchange membranes (IEMs) in the presence of an electric field. When a potential is applied between two electrodes, anions are transported towards the anode through positively charged anion exchange membranes (AEMs), and cations are transported towards the cathode through negatively charged cation exchange membranes (CEMs) [2]. An advantage of ED over reverse osmosis (RO) is a higher water recovery as ED is not limited by brine osmotic pressure [3,4]. Additionally, ED is reported to be more economical than RO and thermal desalination technologies for the treatment of water with total dissolved solids (TDS) below 5,000 $mg \cdot L^{-1}$[5].

Fouling is defined as one of the main limitations hindering a greater use of membrane processes [6]. Fouling consists in the undesired attachment of living organism or non-living substances to membrane surface or membrane structure [7]. This important issue affects membrane desalination technologies such as RO [8], membrane distillation [9,10] and ED [11,12]. Fouling affecting ion exchange membranes can be classified into colloidal fouling, organic fouling, scaling and biofouling [7]. The nature and state of the substance producing fouling or *foulant* determines the fouling classification. Colloidal fouling is generated by non-dissolved suspended solids or colloids. Organic dissolved substances cause organic fouling. Scaling is caused by dissolved salts and biofouling by live organisms. Regarding organic fouling and ED, the organic salts that usually produce fouling on IEMs are formed by a large anion that is a foulant for AEMs and a small cation that passes through the CEMs [13]. Thus, because most organic foulants are negatively charged, this phenomenon mainly affects AEMs [12], which makes choosing AEMs with high fouling resistance essential [14]. AEMs are also reported to be more susceptible to fouling by natural organic matter than CEMs [15]. Some strategies for fouling prevention and mitigation of IEMs are the use of cleaning agents [16], pretreatment of solutions [17-19], mechanical removal [20], control of the hydrodynamic conditions [21], use of electrodialysis with reversal polarity [22,23] and pulsed electric field [24,25]. Fouling is a widely studied issue in membrane development for pressure driven desalination processes but they are only a few works about fouling resistant ion exchange membranes. One of the most important strategies for fouling prevention in membrane development is the modification of the membrane surface [7,26,27]. In the particular case of IEMs, the modification of surface physicochemical characteristics can include surface charge, hydrophobic/hydrophilic balance and roughness [7]. The modification of surface charge promotes electrostatic repulsion between charged foulants and membranes. The increase of membrane surface hydrophilicity avoids hydrophobic interactions of foulants and the membrane surface [26]. Smooth surfaces reduce the contact area for fouling attachment to the membrane surface [27]. Some examples of membrane surface modification techniques for fouling mitigation in IEMs involve the use of membrane sulfonating agents [26], layer by layer deposition [28]

[29], immersion [30] or direct casting [31]. The use of nanomaterials plays a key role in membrane surface modification of pressure driven desalination processes for fouling and biofouling prevention and mitigation [6,32,33]. Carbon-based nanomaterials, in particular carbon nanotubes, are attracting special attention due to their flexibility, good mechanical properties, good electrical conductivity, easy scale-up, high purity and low production cost [6,34-37]. However, only one work can be found in the literature regarding the use of nanomaterials for fouling resistant IEMs. Particularly, carbon nanotubes (CNTs) for fouling resistant cation exchange membranes were used in [38]. This previous study reports very promising fouling resistant membranes for power generation by reverse electrodialysis.

The authors of the present work support these previous findings in fouling resistant nanocomposite IEMs and supplement them by comparing the performance of two nanomaterials with a totally different geometry: 1) one-dimensional oxidized multi-walled carbon nanotubes CNTs-COO^- (CNTs) and 2) zero-dimensional sulfonated iron oxide nanoparticles Fe_2O_3-SO_4^{2-} (NPs) in enhancing fouling resistance of AEMs. The classification of nanomaterials into zero-dimensional and one-dimensional is based on the number of dimensions that do not belong to the nanoscale range. Nanoparticles are zero-dimensional nanomaterial as their only dimension, the diameter, belongs to the nanoscale range. On the other hand, carbon nanotubes are a typical example of one-dimensional nanomaterial as their diameters is usually in the nanoscale range, but not their length. A complete classification of nanomaterials according to their dimensions can be found elsewhere [39].

In our previous study [40] commercially available heterogeneous polyethylene AEMs were modified by direct casting of a solution that combines Fe_2O_3-SO_4^{2-} nanoparticles with sulfonated poly (2,6-dimethyl-1,4-phenylene oxide) (sPPO). This coating introduced a very thin negatively charged layer on the surface of the AEMs providing them with monovalent selectivity. The most important findings of this previous work were: 1) The monovalent selectivity of nanocomposite membranes remained steady with long operation times in electrodialysis with bipolar membranes (up to 93 hours of operation) and 2) the nanocomposite thin film was stable even when working with strong acids and bases. This stability is highly desired in electrodialysis when working with bipolar membranes [41].

The objective of this work is to evaluate effects produced by the introduction of this negatively charged nanocomposite layer on the fouling resistance of polyethylene AEMs. Two different nanocomposite layers were used: 1) sPPO and Fe_2O_3-SO_4^{2-} (used as nanocomposite film in our previous work) and 2) sPPO and CNTs. Due to the nature of the sPPO film, the functionalized nanomaterials, and direct casting (as the chosen technique), the treatment provided the membrane surface with negative charges, high hydrophilicity and a smooth surface that significantly improved membrane fouling resistance. The hydrophilic character of sPPO, Fe_2O_3-SO_4^{2-} and CNTs-COO^- was reported elsewhere [38,42-45]. The use of sPPO, Fe_2O_3-SO_4^{2-} and CNTs-COO^- allowed a highly negative charge within a very thin layer. Thus, it improved conductivity and

reduced the resistance of the negative layer that has been reported to contribute significantly to the total resistance of the membrane in other studies about membrane surface modification [30],[46].

2. Experimental

2.1. Materials

Commercial heterogeneous polyethylene AEMs (Ralex AM-PP) (Mega, Czech Republic) were subjected to modification. Ralex AM-PP membranes are conventional membranes for ED widely used in different electrodialysis processes [47-49]. Some of the most attractive characteristics of AM-PP membranes are low price, long life cycle and long-term stability at pH 0-14 which made them good candidates for our previous study [40]. Poly (2,6-dimethyl-1,4-phenylene oxide) (PPO) (analytical standard grade), chloroform (anhydrous, 99% wt), methanol (anhydrous, 99.8% wt), chlorosulfonic acid (99% wt) and sulfuric acid (98% wt) were purchased from Sigma Aldrich (St. Louis, USA). Dimethyl sulfoxide (DMSO) (ACS grade, 99.9% wt) was obtained from VWR (Atlanta, USA). Iron (III) oxide nanoparticles (Ø50 nm, Sigma Aldrich) were used as received for sulfonation. Oxidized multi-walled carbon nanotubes with an outer diameter of < 8 nm, a length of 10 µm –30 µm and a carboxyl group content of 3.86 % wt were purchased from Cheap Tubes (Cambridge, USA) (purity 95% wt) and used as received. Sodium dodecyl sulfate (SDS, Sigma Aldrich) was used as a model organic foulant.

2.2. Surface modification of polyethylene anion exchange membrane

This work modifies the surface of a commercial polyethylene AEMs by a physical coating [50] using sPPO and Fe_2O_3-SO_4^{2-} or sPPO and CNTs-COO^-. The modification of polyethylene membranes was performed only in the layer facing the dilute compartment, the one where the concentration of ions decreases. This was done for the following reasons: 1) lower current efficiencies in the desalination process have been reported when the modified surface was facing the concentrate compartment [51] and 2) since negative charges of the membrane surface may attract Na^+ cations, only the side that is in the opposite direction to the flux of cations in the cell (towards the cathode as shown in Figure 1) was modified in order to avoid a loss of Cl^-/Na^+ permselectivity.

PPO and Fe_2O_3 sulfonation was carried out according to a procedure described in [42,43]. The sulfonation of PPO was performed by using chloroform and methanol as solvents and chlorosulfonic acid as the sulfonating agent. Fe_2O_3 powder nanoparticles were sulfonated by contact with a concentrated solution of sulfuric acid followed by calcination at 500 ºC.

An exhaustive cleaning of the polyethylene membrane surface was done before surface modification. The membrane was submerged in a solution 0.1 $mol \cdot L^{-1}$ HCl, rinsed with deionized water and submerged in a 0.1 $mol \cdot L^{-1}$ NaOH solution. This procedure was repeated at least three times. After the pretreatment, the membrane was dried at room temperature. The modification of the membrane surface was done using a solvent-evaporation technique [52]. A PPO and DMSO solution of 19% $g \cdot g^{-1}$ was mixed with

different loadings of nanomaterials at 40 ºC and continuously stirred for 24 hours. The solution was then vibrated for 10 minutes for optimal dispersion of the nanomaterials. After that, the solution was cast onto the commercial membrane using the doctor blade method. The obtained nanocomposite membranes were dried in a vacuum oven at 60 ºC for 24 hours. The membranes were treated with 1 $mol \cdot L^{-1}$ HCl for 24 hours, rinsed in deionized water and stored in a solution 0.5 $mol \cdot L^{-1}$ NaCl. Table 1 includes a summary of the nanocomposite membranes obtained and the loading of nanomaterials used in this work. The loadings and compositions of NPs coated membranes, AM-0.2NP, AM-0.4NP and AM-0.6NP, are the same as the ones used in our previous work on valorization of desalination brines into acids and bases by electrodialysis with bipolar membranes [40].

Table 1. Summary of nanocomposite ion exchange membranes synthetized in this work.

Name	Composition of the layer	Loading of nanomaterial (% $g \cdot g^{-1}$*)
AM-0.2NP	SPPO, Fe_2O_3-SO_4^{2-}	0.2
AM-0.4NP	SPPO, Fe_2O_3-SO_4^{2-}	0.4
AM-0.6NP	SPPO, Fe_2O_3-SO_4^{2-}	0.6
AM-0.2CNTs	SPPO, CNTs-COO^-	0.2
AM-0.4CNTs	SPPO, CNTs-COO^-	0.4
AM-0.6CNTs	SPPO, CNTs-COO^-	0.6
AM-0.8CNTs	SPPO, CNTs-COO^-	0.8

*g nanomaterial · g^{-1} layer.

2.3. Membrane characterization

2.3.1. FTIR spectra analysis

The chemical composition of unmodified and nanocomposite AEMs was determined by Digilab FTS7000 Fourier Transform Infrared Spectroscopy (FTIR) (Randolph, MA, USA) equipped with a Digilab UMA600 microscope. Spectra were scanned in a range of 700 cm^{-1} - 4000 cm^{-1} at a resolution of 4 cm^{-1}. For each sample, the scan was repeated 20 times. Results were corrected using a spectrum of ambient air as a background.

2.3.2. Scanning electron microscopy (SEM) analysis

Surface and cross-sectional morphology was studied using a Hitachi SU8230 cold field emission scanning electron microscope (CFE-SEM) (Tarrytown, NY, USA). Samples were dried at 60 ºC for at least 24 hours before testing.

2.3.3. AFM analysis

Keysight 5500 Molecular Imaging Atomic Force Microscope (AFM) (Keysight Technologies, USA) was used to analyze surface morphology. An area of 50 µm by 50 µm on each sample was scanned in the acoustic alternating current (AAC) mode using silicon cantilevers (Budget Sensors, Bulgaria). Picoview 1.12 software from Keysight

Technologies (formerly Agilent) was used to process scanned images and generate morphological parameters.

2.3.4. Water contact angle

Dried samples were placed on a Ramé-Hart Model 250 goniometer (Succasunna, USA) for contact angle measurement using deionized water. At least three measurements were conducted for each sample.

2.3.5. Membrane resistance

Membrane resistance was measured using electrochemical impedance spectroscopy (EIS) in a two-compartment cell experimental setup shown in Figure 1 with a 0.5 $mol \cdot L^{-1}$ NaCl solution. Oscillating voltages with an amplitude of 25 mV were applied by means of a Vertex potentiostat-galvanostat (Ivium Technologies, Eindhoven, Netherlands). Frequency of the impedance measurements ranged from 0.1 Hz to 1000 Hz. Membrane resistance was determined from the fitting of the response to the equivalent circuit for ion exchange membranes with solutions reported in [53]. Because of the fitting, a global parameter that includes membrane resistance and solution resistance (R_{M+S}) was obtained. This value was corrected by measuring the resistance of the solution in a blank experiment without the membrane.

2.4. Evaluation of fouling resistance

The evaluation of the fouling resistance of unmodified and nanocomposite membranes was performed by chronopotentiometry in the experimental setup shown in Figure 1. The two-compartment cell was filled with a solution of 0.1 $mol \cdot L^{-1}$ NaCl and 0.0018 $mol \cdot L^{-1}$ SDS as the model foulant. Each compartment has a volume of approximately 0.2 L. The experiments were run for 100 minutes. The modified surface of the membrane was set facing the dilute compartment. The applied current density was 2 $mA \cdot cm^{-2}$ being the effective area of the membrane 4.8 cm^2. Fouling causes an increase in membrane resistance and thus an increase in the voltage drop through the membrane (ΔV). The fouling resistance of membranes was determined by measuring the evolution of ΔV with time using Luggin capillaries. Polyethylene membranes (Ralex AM-PP) and the best nanocomposite membrane were subjected to three 4-hour operation cycles with the model fouling solution. Membranes were rinsed with deionized water between cycles. The energy consumption during these cycles was calculated from the area of ΔV-t curves using the trapezoidal rule.

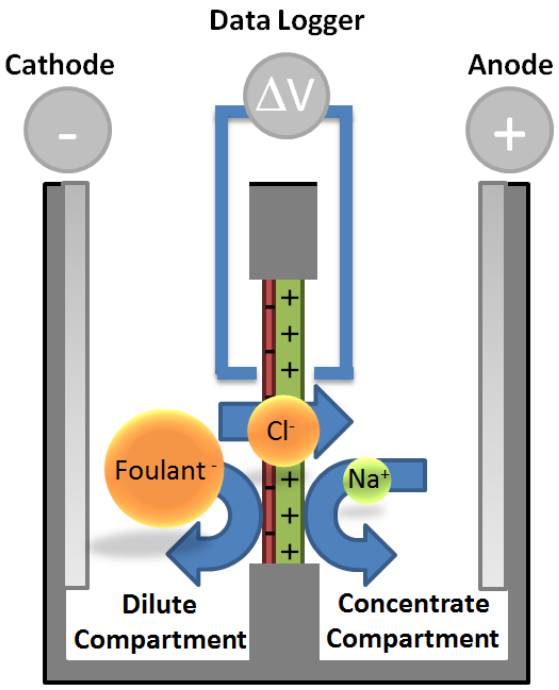

Figure 1. Scheme of the experimental setup used to determine membrane resistance and fouling resistance.

3. Results and discussion

3.1. Surface membrane composition

Figure 2 shows the FTIR spectra of unmodified and nanocomposite AEMs. The characteristic peak of C-H stretch in $–CH_2–$ and $CH_3–$ substitutes, corresponding to polyethylene and polypropylene of the AM-PP membranes, were observed at 2,918 cm^{-1} and 2,850 cm^{-1} respectively [54]. The transmittance band at 1,170 cm^{-1} was assigned to the C-O-C stretch of sPPO [54]. The presence of the $–SO_3H$ substitute in the aromatic ring of PPO was confirmed by a peak at 1,062 cm^{-1} [42]. FTIR spectra confirmed the success in coating the commercial membrane with the negatively charged thin film of sPPO and nanomaterials.

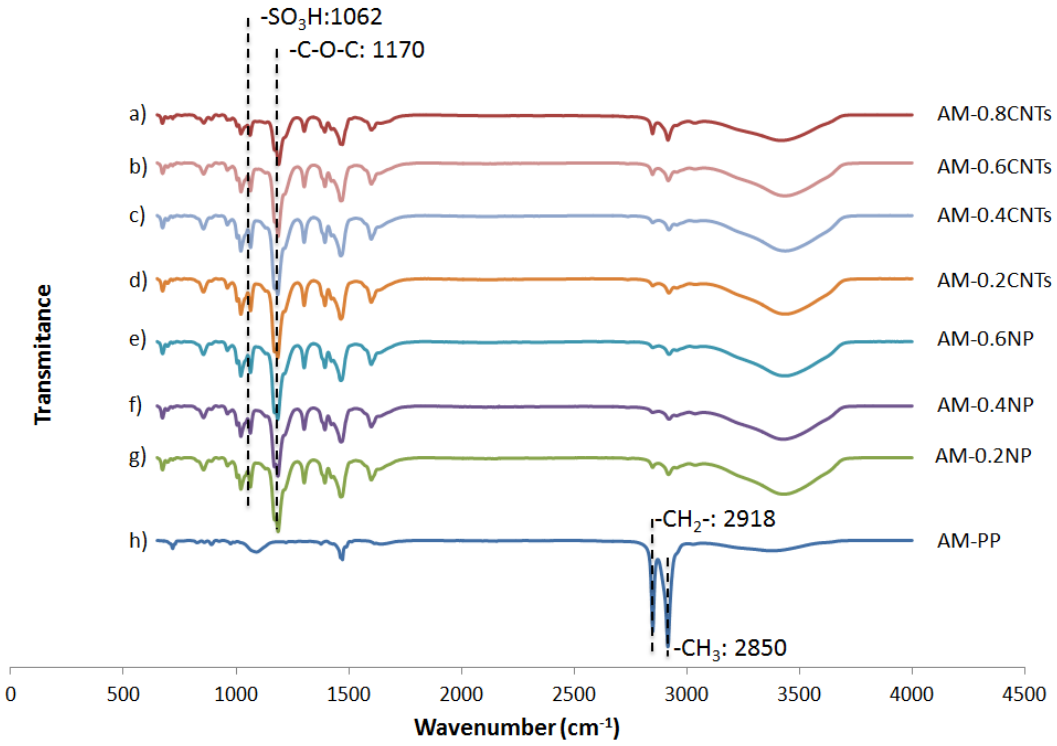

Figure 2. FTIR spectra of anion exchange membranes a) AM-0.8CNTs, b) AM-0.6CNTs, c) AM-0.4CNTs, d) AM-0.2CNTs, e) AM-0.6NP, f) AM-0.4NP, g) AM-0.2NP and h) Ralex AM-PP (unmodified membrane).

3. 2. Membrane morphology

Scanning electron microscopy (SEM) was used to observe the morphology of unmodified and nanocomposite AEMs. Figure 3a shows SEM images of surface and cross-section of Ralex AM-PP membranes, heterogeneous AEMs reinforced with polypropylene fibers. It can be clearly seen in these images that the fibers are distributed in the membrane matrix forming a uniform square grid parallel to its surface (Figure 3a.1). From the cross-section images (Figure 3a.3 and Figure 3b.3), it can be concluded that there are two levels of fibers distributed homogeneously. This reinforcement provides the membrane with a very good mechanical stability and robustness but also a heterogeneous conductivity.

From the comparison of the SEM images for the unmodified membrane (Figure 3a) and the nanocomposite membrane AM-0.2NP (Figure 3b), an improvement can be seen in the surface homogeneity with membrane coating. This hypothesis was confirmed by atomic force microscopy (AFM), as will be discussed later. Cross-section images (Figure 3a.3 and Figure 3b.3) were used to determine the thickness of unmodified membranes (485 μm), and the thin film of nanocomposite membranes (19 μm). These results confirm the small contribution of the coating to the total thickness of the membrane (increase below 4%).

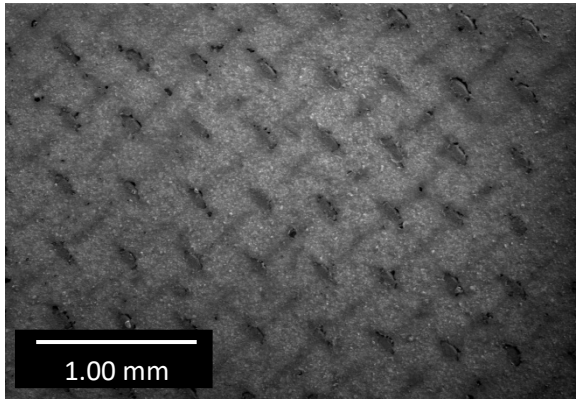

Figure 3a.1 Surface of unmodified membrane Ralex AM-PP at 1 mm

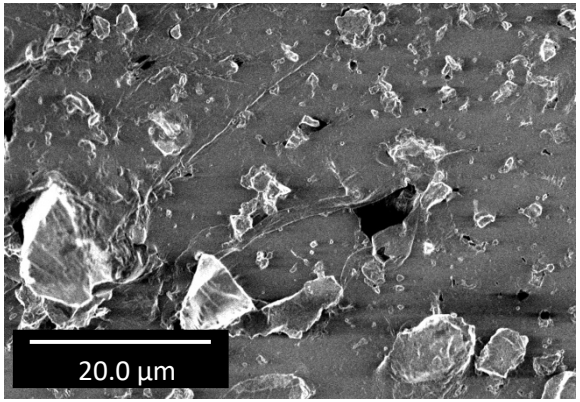

Figure 3a.2 Surface of unmodified membrane Ralex AM-PP at 20 µm

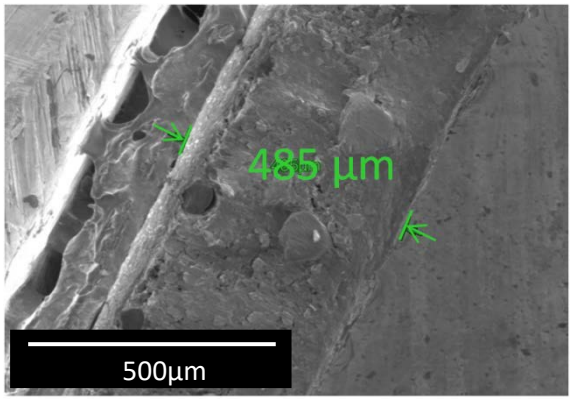

Figure 3a.3 Cross-section of unmodified membrane Ralex AM-PP at 500 µm

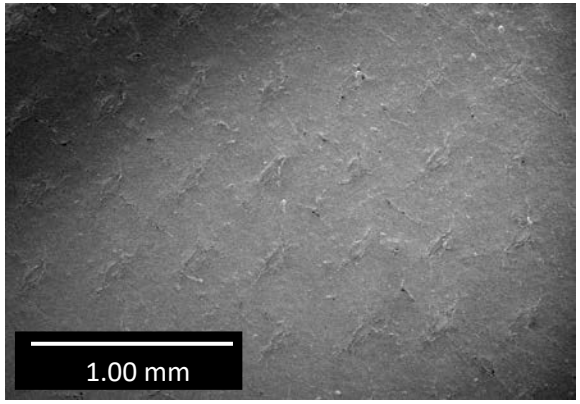

Figure 3b.1 Surface of nanocomposite membrane AM-0.2NP at 1 mm

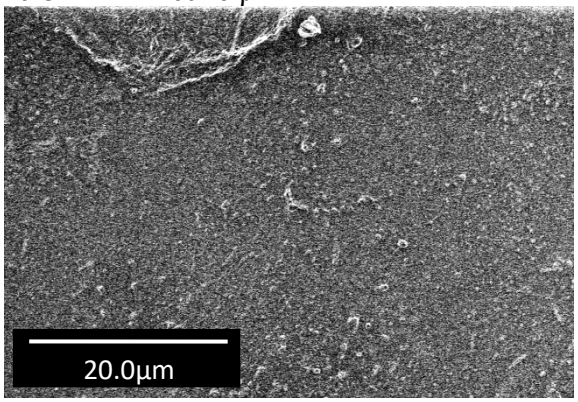

Figure 3b.2 Surface of nanocomposite membrane AM-0.2NP at 20 µm

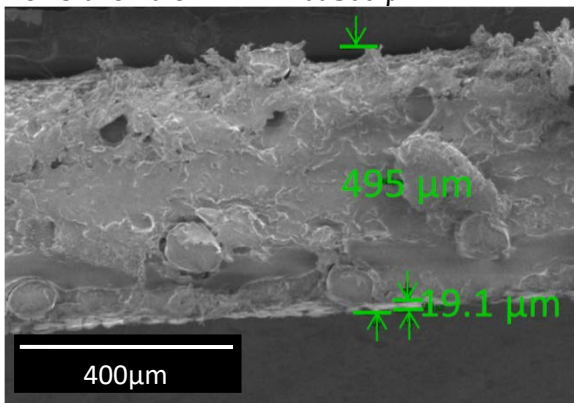

Figure 3b.3 Cross-section of nanocomposite membrane AM-0.2NP at 400 µm

Figure 3. SEM images for unmodified membrane Ralex AM-PP a. 1-3 and nanocomposite membrane AM-0.2NP b. 1-3.

3. 3. Membrane roughness

Modifications of membrane roughness with the coating, directly related to surface homogeneity, were determined by AFM. The membrane characterization was performed by means of three different morphological parameters displayed in Table 2 as 1) Sq (root mean square height), which is the standard deviation of the height distribution, also referred to as RMS surface roughness, 2) Sp (maximum peak height), which is the height between the highest peak and the mean plane of the surface, and 3) Sv (maximum pit height), which is defined as the depth between the mean plane of the surface and the deepest valley.

Membranes Ralex AM-PP presents a rough surface with a Sq of 702 nm. This roughness might be beneficial for the static adhesion between the commercial membrane and the nanocomposite thin film as rough surfaces result in a higher contact area [31]. The data presented in Table 2 and the 3D AFM images of Figure 4 confirm the decrease of membrane surface roughness with the coating. Table 2 shows that all the morphological parameters that describe surface roughness are significantly lower for nanocomposite membranes than for the unmodified membrane, and thus, the membrane roughness decreased with the nanocomposite layer. Nanocomposite membranes modified with carbon nanotubes presented a surface slightly rougher than the ones modified with iron oxide nanoparticles. Sq decreased 36% to 77% in the case of NPs, and 28% to 58% when membranes are modified with CNTs. The incorporation of sPPO and nanomaterials made the surface of the membrane smoother because the coating might be accumulated in the valleys [31]. This is in agreement with the decreases in the height of the highest peak and the depth of the deepest valley (Sp and Sv, respectively) observed in the nanocomposite membranes. The apparent smoothness of the nanocomposite membranes was also observed in the SEM images of Section 3.1.2. *Membrane morphology*. A decrease of surface roughness was also reported when modifying a commercial AEMs by casting [31]. On the contrary, the use of layer by layer deposition [29] and immersion [55][46] has showed a significant increase of membrane roughness, making the surface rougher when increasing the number of layers [29] and the concentration of polymer [46].

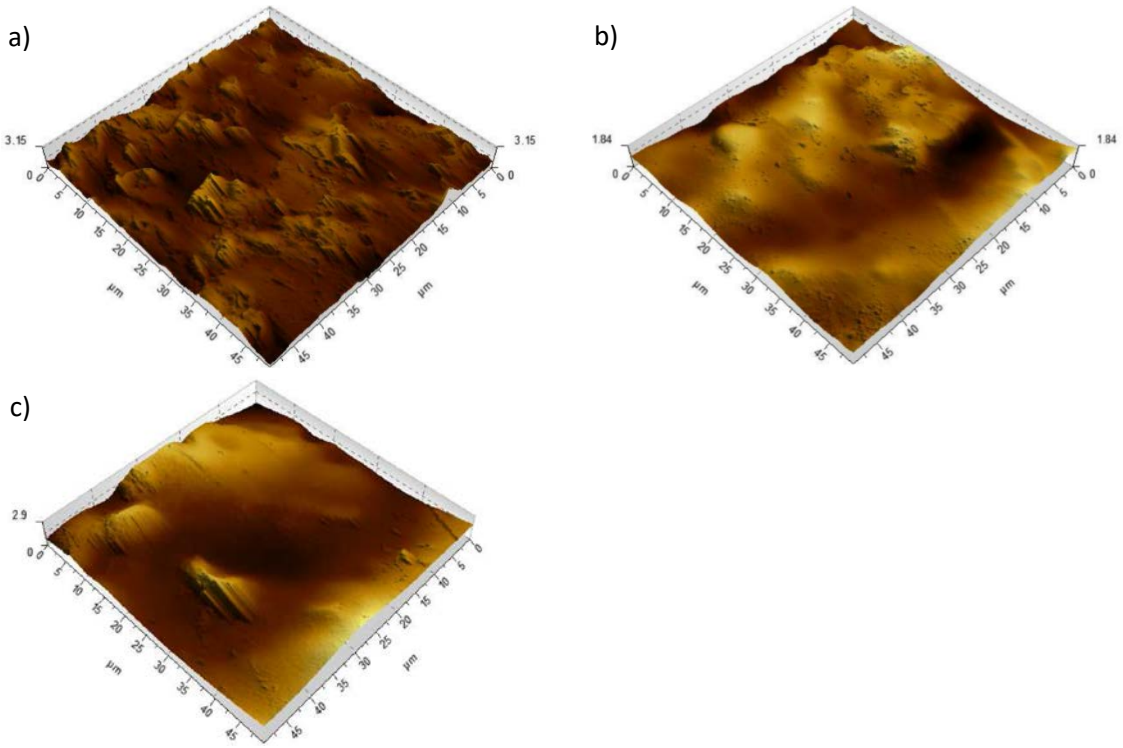

Figure 4. AFM 3D images of surface roughness for a) unmodified membranes AM-PP, b) nanocomposite membranes AM-0.2NP and c) nanocomposite membranes AM-0.6CNTs

Table 2. Summary of morphological parameters of unmodified and nanocomposite membranes expressed in nm.

Membrane	Sq (nm)	Sp (nm)	Sv (nm)
AM-PP	702	2410	2090
AM-0.2NP	297	917	930
AM-0.4NP	160	773	448
AM-0.6NP	256	953	1060
AM-0.2CNTs	317	1180	949
AM-0.4CNTs	301	2090	1080
AM-0.6CNTs	506	1700	1240
AM-0.8CNTs	373	2290	824

3. 4. Membrane hydrophilicity

One of the most important parameters regarding fouling phenomena and membrane resistance in desalination processes is membrane hydrophilicity [7] [56] evaluated by WCA measurements. The introduction of nanomaterials on membranes can modify its physicochemical properties such as hydrophilicity [50]. Water contact angle measurements of Ralex AM-PP membranes and nanocomposite membranes are presented in Table 3. Figure 5 illustrates how the modification of the membrane surface

showed a significant increase in membrane hydrophilicity and thus, a decrease in the water contact angle. Ralex AM-PP membranes are very hydrophobic as they present a water contact angle of 100.1º. These high values have also been reported in other heterogeneous anion exchange membranes [29]. In the case of Ralex AM-PP membranes, based on polyethylene and polypropylene, the high-water contact angle might be due to the high presence of PP and PE on the surface, making the membrane water contact angle very close to the water contact angle of pure PE and PP, 94º and 97º, respectively [57]. A high content of polyethylene in the surface of heterogeneous membrane has also been reported in [58].

The introduction of sPPO and Fe_2O_3-SO_4^{2-} nanoparticles on the membrane surface caused a decrease of 36º–39º in the water contact angle of nanocomposite membranes. This decrease in water contact angle is probably due to the high hydrophilicity and the large specific area of Fe_2O_3-SO_4^{2-} nanoparticles [42] and to the increase of functional groups associated with the negative charge layer (sulfonic acid and sulfate groups) [31,44]. In the case of membranes modified with CNTs, the drop-in water contact angle is even higher, 37º–42º and due to the increase of negatively charged carboxyl groups on the surface of the CNTs [38] and sulfonic acid groups of sPPO. The WCA of the membranes modified with CNTs (57.9º–62.9º) is in agreement with WCA reported for nanocomposite cation exchange membranes made of sPPO and CNTs functionalized with COO^- for power generation by reverse electrodialysis (50.8º–75.9 for a loading between 0.1% $g \cdot g^{-1}$ and 0.8% $g \cdot g^{-1}$ CNTs [38]). The decrease of water contact angle in all of the nanocomposite membranes is translated into a higher fouling resistance to be discussed in Section 3.6. *Membrane fouling resistance*. The most hydrophilic nanocomposite membranes were AM-0.4NP for iron oxide nanoparticles and AM-0.6CNTs in the case of carbon nanotubes. These membranes also showed the best fouling resistance as later discussed.

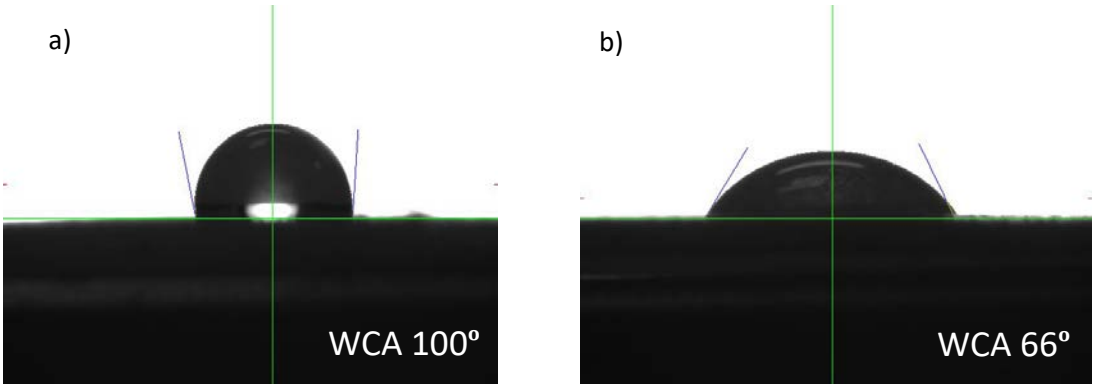

Figure 5. Water contact angle of a) a membrane Ralex AM-PP and b) a nanocomposite membrane AM-0.6NP.

Table 3. Summary of water contact angles of unmodified and nanocomposite anion exchange membranes.

	Contact angle (º)	Contact angle decrease (º)
AM-PP	100.1±3.2	-
AM-0.2NP	63.7±3.4	36
AM-0.4NP	61.6±3.4	39
AM-0.6NP	65.8±0.9	34
AM-0.2CNTs	59.7±6.3	40
AM-0.4CNTs	62.9±2.8	37
AM-0.6CNTs	57.9±2.3	42
AM-0.8CNTs	60.7±5.0	39

3.5. Membrane electrical resistance

The energy consumption of an ED process is related to the resistance of the solutions and IEMs [59]. Thus, membranes with low electric resistance are preferable for operating with ED. Electric resistance of membranes depends on several factors such as membrane thickness [60] and water content [56]. From the results presented in Table 4, it can be concluded that the surface resistance of the modified AEMs in this work did not change after the coating. This could be due to the following reasons: 1) the thickness of the layer added to the membrane is very small (19 μm, from SEM images of Figure 3b) when compared to the thickness of the unmodified membrane (485 μm, from SEM images of Figure 3a); 2) the introduction of nanomaterials allows a high negative charge in a very thin layer. Although adding a new layer to the membrane surface would theoretically increase membrane resistance, the resistance of this layer is expected to decrease with increasing negative charge density and the resistance is not expected to increase drastically [61], and 3) the negative layer is very hydrophilic. Water content and membrane hydrophilicity also have an important impact on membrane resistance. The ionic resistance of a membrane decreases dramatically when increasing water content [56]. Thus, the increase in surface hydrophilicity after coating the membrane (see Figure 5 and Table 3) supports the hypothesis of high sPPO and functionalized nanoparticles' layer hydrophilicity, thereby achieving high water affinity of the layer and low electrical resistance. Additionally, the direct casting allows the modification of only one of the two sides of the membranes, reducing by half the potential resistance increase with the treatment (as only one layer is introduced on one of the sides of the membrane surface, instead of both sides).

A significant increase of membrane hydrophilicity when using iron oxide nanoparticles and carbon nanotubes has already been reported [38,42]. Thus, the contribution of the negative layer to the total resistance of the membrane is very low and does not affect the total ionic resistance of nanocomposite membranes. No significant changes regarding

membrane resistance after modification by casting have been reported for heterogeneous AEMs [58].

Finally, some differences in membrane resistance have been reported when adding a negatively charged layer. The changes of membrane resistance ranged from slightly positive increments in the case of modification by direct casting (0.93 $\Omega \cdot cm^2$ to 1.1 $\Omega \cdot cm^2$ [31]) and layer by layer deposition (4.47 $\Omega \cdot cm^2$ to 4.81 $\Omega \cdot cm^2$ [29]) to relevant for immersion (from 2.5 $\Omega \cdot cm^2$ to 5.0 $\Omega \cdot cm^2$ [46]). Thus, the increase of membrane resistance might also be highly influenced by the selected modification method.

Table 4. Membrane resistance for unmodified and nanocomposite anion exchange membranes. A solution 0.5 $mol \cdot L^{-1}$ NaCl was used as electrolyte.

Membrane	Surface Resistance ($\Omega \cdot cm^2$)
AM-PP (as reported by supplier)	< 8
AM-PP	6.3±0.12
AM-0.2NP	6.1±0.04
AM-0.4NP	6.1±0.04
AM-0.6NP	6.4±0.03
AM-0.2CNTs	6.2±0.01
AM-0.4CNTs	6.4±0.04
AM-0.6CNTs	6.8±0.02
AM-0.8CNTs	6.3±0.08

3.6. Membrane fouling resistance

Fouling is defined as one of the key problems for food processing and water treatment [7]. Membrane modification can lead to very promising advantages regarding fouling prevention such as less power consumption and a lower pretreatment cost [7]. The most common method to estimate membrane stability against fouling is measuring the change in the voltage drop across the membrane [62]. Figure 6 includes the evolution of ΔV for all nanocomposite membranes and the Ralex AM-PP membrane. From this figure it can be observed that all nanocomposite membranes have a better fouling resistance than the unmodified membrane. Nanocomposite membranes modified with CNTs showed a slightly better performance. To quantify the improvement in fouling resistance of nanocomposite membranes, Table 5 includes the evolution of the voltage drop with time as $V \cdot min^{-1}$. Figure 7 shows the improvement of fouling resistance in % defined for each of the nanocomposite membranes *i* as $Improvement_i$ in Eq. 1. $\Delta V_{Nanocomposite_i}$ is the slope of the different nanocomposites AEMs presented in Table 5 and $\Delta V_{Unmodified}$ is the slope of the unmodified Ralex AM-PP membrane of Table 5.

$$Improvement_i = \left(1 - \frac{\Delta V_{Nanocomposite_i}}{\Delta V_{Unmodified}}\right) \cdot 100 \qquad \text{Eq. 1}$$

The introduction of the negatively charged hydrophilic layer supposed an improvement of fouling resistance that varied between 25% and 53% expressed as a decrease in the slope of ΔV vs time. The optimum loadings of nanocomposite membranes were 0.4% for Fe_2O_3-SO_4^{2-} nanoparticles and 0.6% for O-MWCNTs. These membranes also showed the highest hydrophilicity (see Table 3). The decrease in performance after the optimum dose of CNTs and NPs is probably due to the aggregation of nanomaterials in the thin layer. A homogeneous dispersion of nanomaterials in the polymer matrix is essential to transfer their properties to the nanocomposite layer [63].

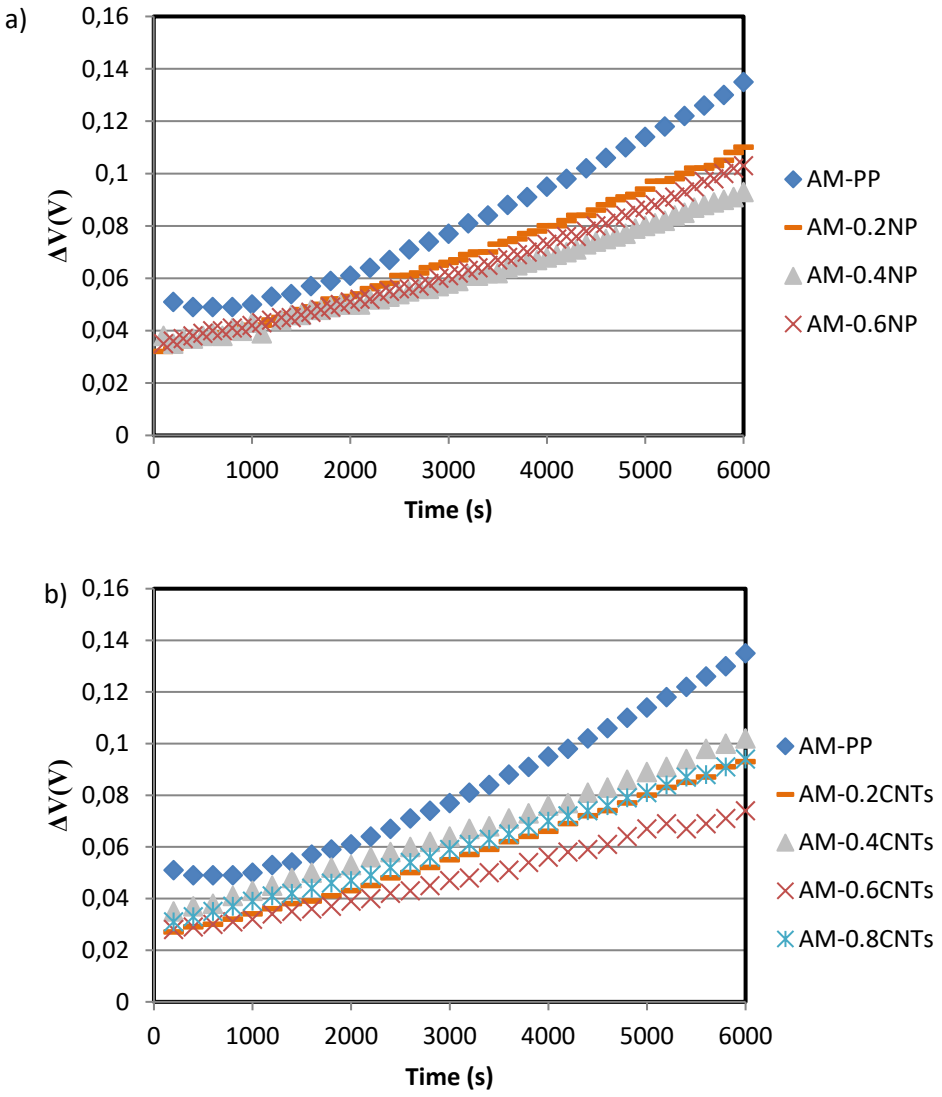

Figure 6. Evolution of voltage drop across the membrane (ΔV) for different AEMs: a) unmodified AM-PP, AM-0.2NP, AM-0.4NP and AM-0.6NP and b) unmodified AM-PP, AM-0.2CNTs, AM-0.4CNTs, AM-0.6CNTs, and AM-0.8CNTs. Current density was 2 $mA \cdot cm^{-2}$. Solution 0.1 $mol \cdot L^{-1}$ NaCl and 0.0018 $mol \cdot L^{-1}$ SDS.

Table 5. Slope of the evolution of the voltage drop with time for the different AEMs shown in Figure 6.

Membrane	slope ($mV \cdot min^{-1}$)
AM-PP	1.04*
AM-0.2NP	0.78
AM-0.4NP	0.58
AM-0.6NP	0.68
AM-0.2CNTs	0.69
AM-0.4CNTs	0.69
AM-0.6CNTs	0.49
AM-0.8CNTs	0.65

*The slope was calculated using the data from 1000 seconds to 6000 seconds.

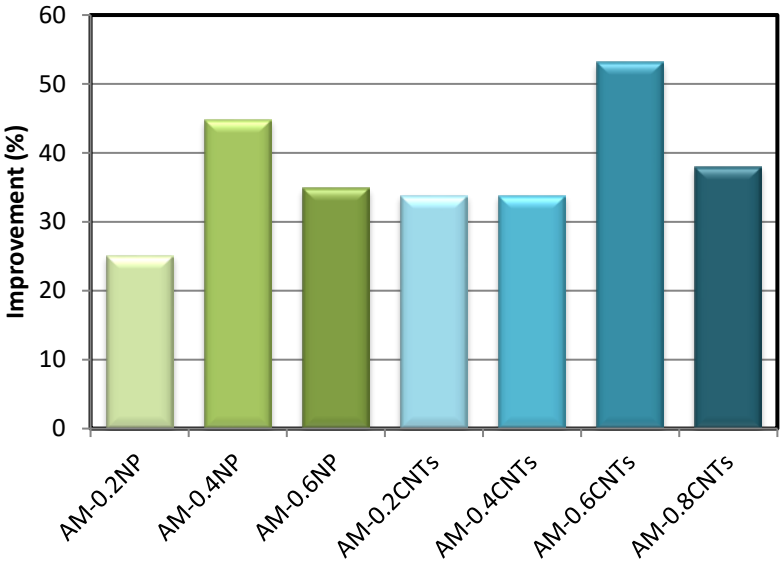

Figure 7. Improvement of the fouling resistance of nanocomposite membranes.

Additional experiments were performed with the best nanocomposite membrane, AM-0.6CNTs being compared to the unmodified Ralex AM-PP membrane. In these experiments AM-PP and AM-0.6CNTs membranes were subjected to three 4-hour cycles of operation. Figure 8 includes the results of these experiments, which show that the difference in fouling resistance between the nanocomposite AM-0.6CNT membranes and the Ralex AM-PP membranes remained almost constant, even after 12 hours of operation.

The main reason behind the improvement of this fouling resistance relies on the modification of three characteristics of membrane surfaces with significant influence over anti-fouling properties: membrane charge, surface roughness and hydrophilicity [32]. SEM and AFM images (Figure 3 and Figure 4, respectively) verify the improvement in the homogeneity of nanocomposite membranes. Nanocomposite membranes, with smoother surfaces than commercial membranes as previously presented had significantly lower fouling rates [64],[27]. The surface hydrophilicity of

nanocomposite membranes was observed in the water contact angle measurements (as shown in Table 3 and Figure 5). All of these modifications to membrane surface physicochemical characteristics provided nanocomposite membranes with enhanced antifouling properties in the presence of SDS as a model organic foulant. This fouling resistance was probed to be maintained with time. It is noteworthy that two nanomaterials, which are different in geometry and functionalization, can have such a similar performance and improvement in a very close loading (0.2% $g \cdot g^{-1}$–0.6% $g \cdot g^{-1}$ for iron oxide nanoparticles and 0.2% $g \cdot g^{-1}$–0.8% $g \cdot g^{-1}$ for CNTs). These similarities were first observed during the characterization process and then confirmed in the evaluation of the fouling resistance. Nanocomposite membranes using CNTs performed slightly better in fouling resistance and surface hydrophilicity. This might be due to a slightly higher loading of nanomaterials before the aggregation processes.

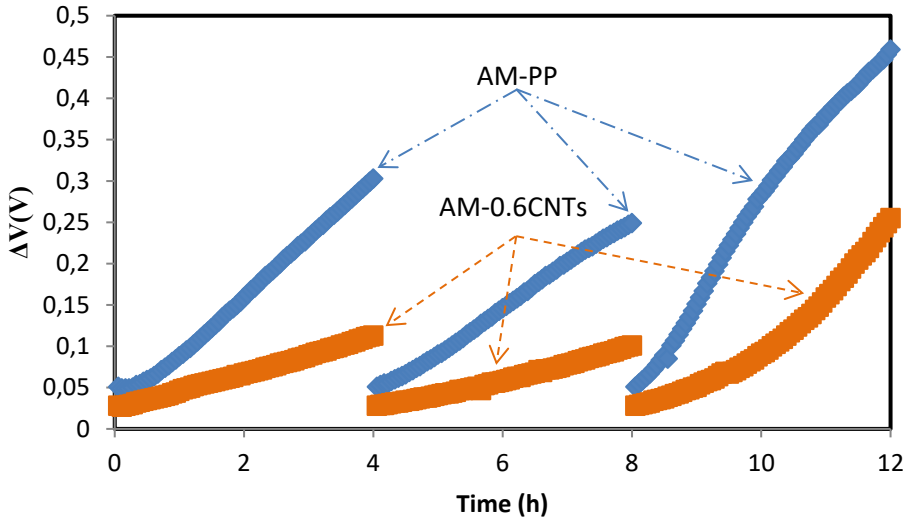

Figure 8. Evolution of voltage drop across the membrane (ΔV) for polyethylene membranes AM-PP and nanocomposite membranes AM-0.6CNTs during three 4-hour cycles of operation. Current density was 2 $mA \cdot cm^{-2}$.

The energy consumption using the unmodified Ralex AM-PP membrane and the best nanocomposite membranes AM-0.6CNTs was calculated from the area under the curves of Figure 8. The energy consumption decreased by 59.7% in the first cycle, 57.5% in the second and 48.5% in the third cycle. These promising results give an idea of the potential energy savings of a process that uses nanocomposite membranes with fouling resistant properties.

4. Conclusions

This work presents the performance in terms of fouling resistance of novel nanocomposite anion exchange membranes based on a polyethylene commercial anion exchange membrane and a thin nanocomposite layer. This layer is composed of sPPO and one nanomaterial: one-dimensional oxidized multi-walled carbon nanotubes CNTs-COO^- or zero-dimensional sulfonated iron oxide nanoparticles Fe_2O_3-SO_4^{2-}, each with a totally different geometry and composition. The introduction of this layer caused a significant change in some physicochemical characteristics of the membrane surface such as composition, hydrophilicity and roughness that led to an enhancement of their fouling resistance. All the nanocomposite membranes showed a more hydrophilic and homogeneous surface than the unmodified membranes. The two nanomaterials presented similar performance, observed during the characterization process and then confirmed in the evaluation of the fouling resistance when using similar loadings (0.2% $g \cdot g^{-1}$–0.6% $g \cdot g^{-1}$ for NPs and 0.2% $g \cdot g^{-1}$–0.8% $g \cdot g^{-1}$ for CNTs). However a slightly better performance of nanocomposite membranes using CNTs was observed. It might be due to the fact that CNTs allowed a slightly higher dose of nanomaterials before aggregation. The modification of membrane surface properties was characterized by SEM, FTIR, AMF and water contact angle measurement. The negatively charged layer, with small thickness, high hydrophilicity and conductivity, did not present changes of membrane resistance. The best load of NPs and CNTs was respectively 0.4% $g \cdot g^{-1}$ and 0.6% $g \cdot g^{-1}$ improving fouling resistance by 45% and 53%. These membranes also presented the highest hydrophilicity. The improved fouling resistance of the best nanocomposite membrane AM-0.6CNT was stable during 12 hours of operation in contact with the model foulant. Energy savings between 49% and 60% were achieved due to the lower voltage drop during electrodialysis laboratory scale test. As there is a very similar performance of both nanomaterials, an economic evaluation might be decisive for the selection of the nanocomposite thin film. Further work should explore and compare the effects of different nanomaterials on other transport properties of the membranes, such as flux of ions and permselectivity.

Acknowledgments

Financial support from MICINN under project CTM2014-57833-R and CTQ2013-48280-C3-1-R-D is gratefully acknowledged. The authors thank the Ministry of Education for the FPI grant BES-2012-053461 and the scholarship EEBB-I-15-10268. In addition, this research was partially supported by the U.S. National Science Foundation CBET-1235166.

References

[1] S.E. Kentish, E. Kloester, G.W. Stevens, C.A. Scholes, and L.F. Dumée. Electrodialysis in aqueous-organic mixtures. Separation and Purification Reviews, 44 (2015) 269-282.

[2] M. Kumar, M.A. Khan, Z.A. Al-Othman, and T.S.Y. Choong. Recent developments in ion-exchange membranes and their applications in electrochemical processes for in situ ion substitutions, separation and water splitting. Separation and Purification Reviews, 42 (2013) 187-261.

[3] K. Tado, F. Sakai, Y. Sano, and A. Nakayama. An analysis on ion transport process in electrodialysis desalination. Desalination, 378 (2016) 60-66.

[4] H. Strathmann. Electrodialysis, a mature technology with a multitude of new applications. Desalination, 264 (2010) 268-288.

[5] C. Fernandez-Gonzalez, A. Dominguez-Ramos, R. Ibañez, and A. Irabien. Sustainability assessment of electrodialysis powered by photovoltaic solar energy for freshwater production. Renewable and Sustainable Energy Reviews, 47 (2015) 604-615.

[6] J.H. Jhaveri, Z.V.P. Murthy. A comprehensive review on anti-fouling nanocomposite membranes for pressure driven membrane separation processes. Desalination, 379 (2016) 137-154.

[7] S. Mikhaylin, L. Bazinet. Fouling on ion-exchange membranes: Classification, characterization and strategies of prevention and control. Adv.Colloid Interface Sci., 229 (2016) 34-56.

[8] L. Henthorne, B. Boysen. State-of-the-art of reverse osmosis desalination pretreatment. Desalination, 356 (2015) 129-139.

[9] L.D. Tijing, Y.C. Woo, J. Choi, S. Lee, S. Kim, and H.K. Shon. Fouling and its control in membrane distillation—A review. J.Membr.Sci., 475 (2015) 215-244.

[10] D.M. Warsinger, J. Swaminathan, E. Guillen-Burrieza, H.A. Arafat, and J.H. Lienhard V. Scaling and fouling in membrane distillation for desalination applications: A review. Desalination, 356 (2015) 294-313.

[11] N. Cifuentes-Araya, G. Pourcelly, and L. Bazinet. How pulse modes affect proton-barriers and anion-exchange membrane mineral fouling during consecutive electrodialysis treatments. J.Colloid Interface Sci., 392 (2013) 396-406.

[12] H.-. Lee, M.-. Hong, S.-. Han, S.-. Cho, and S.-. Moon. Fouling of an anion exchange membrane in the electrodialysis desalination process in the presence of organic foulants. Desalination, 238 (2009) 60-69.

[13] D.A. Vermaas, D. Kunteng, M. Saakes, and K. Nijmeijer. Fouling in reverse electrodialysis under natural conditions. Water Res, 47 (2013) 1289-1298.

[14] V. Mavrov, H. Chmiel, B. Heitele, and F. Rögener. Desalination of surface water to industrial water with lower impact on the environment: Part 4: Treatment of effluents from water desalination stages for reuse and balance of the new technological concept for water desalination. Desalination, 124 (1999) 205-216.

[15] K. Bouhidel, M. Rumeau. Ion-exchange membrane fouling by boric acid in the electrodialysis of nickel electroplating rinsing waters: generalization of our results. Desalination, 167 (2004) 301-310.

[16] E. Korngold. Prevention of colloidal-fouling in electrodialysis by chlorination. Desalination, 9 (1971) 213-216.

[17] C. Huang, T. Xu, Y. Zhang, Y. Xue, and G. Chen. Application of electrodialysis to the production of organic acids: State-of-the-art and recent developments. J.Membr.Sci., 288 (2007) 1-12.

[18] E. Vera, J. Ruales, M. Dornier, J. Sandeaux, R. Sandeaux, and G. Pourcelly. Deacidification of clarified passion fruit juice using different configurations of electrodialysis. J.Chem.Technol.Biotechnol., 78 (2003) 918-925.

[19] S.K. Nataraj, S. Sridhar, I.N. Shaikha, D.S. Reddy, and T.M. Aminabhavi. Membrane-based microfiltration/electrodialysis hybrid process for the treatment of paper industry wastewater. Sep.Purif.Technol., 57 (2007) 185-192.

[20] Q. Wang, P. Yang, and W. Cong. Cation-exchange membrane fouling and cleaning in bipolar membrane electrodialysis of industrial glutamate production wastewater. Sep.Purif.Technol., 79 (2011) 103-113.

[21] G. Grossman, A.A. Sonin. Experimental study of the effects of hydrodynamics and membrane fouling in electrodialysis. Desalination, 10 (1972) 157-180.

[22] W.E. Katz. The electrodialysis reversal (EDR) process. Desalination, 28 (1979) 31-40.

[23] Y.-. Chao, T.M. Liang. A feasibility study of industrial wastewater recovery using electrodialysis reversal. Desalination, 221 (2008) 433-439.

[24] H.-. Lee, S.-. Moon, and S.-. Tsai. Effects of pulsed electric fields on membrane fouling in electrodialysis of NaC1 solution containing humate. Sep.Purif.Technol., 27 (2002) 89-95.

[25] S. Suwal, J. Amiot, L. Beaulieu, and L. Bazinet. Effect of pulsed electric field and polarity reversal on peptide/amino acid migration, selectivity and fouling mitigation. J.Membr.Sci., 510 (2016) 405-416.

[26] S. Mulyati, R. Takagi, A. Fujii, Y. Ohmukai, T. Maruyama, and H. Matsuyama. Improvement of the antifouling potential of an anion exchange membrane by surface modification with a polyelectrolyte for an electrodialysis process. J.Membr.Sci., 417–418 (2012) 137-143.

[27] Q. Li, Z. Xu, and I. Pinnau. Fouling of reverse osmosis membranes by biopolymers in wastewater secondary effluent: Role of membrane surface properties and initial permeate flux. J.Membr.Sci., 290 (2007) 173-181.

[28] S. Mulyati, R. Takagi, A. Fujii, Y. Ohmukai, and H. Matsuyama. Simultaneous improvement of the monovalent anion selectivity and antifouling properties of an anion exchange membrane in an electrodialysis process, using polyelectrolyte multilayer deposition. J Membrane Sci, 431 (2013) 113-120.

[29] M. Wang, X. Wang, Y. Jia, and X. Liu. An attempt for improving electrodialytic transport properties of a heterogeneous anion exchange membrane. Desalination, 351 (2014) 163-170.

[30] M. Vaselbehagh, H. Karkhanechi, R. Takagi, and H. Matsuyama. Surface modification of an anion exchange membrane to improve the selectivity for monovalent anions in electrodialysis - experimental verification of theoretical predictions. J.Membr.Sci., 490 (2015) 301-310.

562 [31] E. Güler, W. van Baak, M. Saakes, and K. Nijmeijer. Monovalent-ion-selective membranes
563 for reverse electrodialysis. J.Membr.Sci., 455 (2014) 254-270.

564 [32] V. Kochkodan, N. Hilal. A comprehensive review on surface modified polymer
565 membranes for biofouling mitigation. Desalination, 356 (2015) 187-207.

566 [33] N. Misdan, A.F. Ismail, and N. Hilal. Recent advances in the development of (bio)fouling
567 resistant thin film composite membranes for desalination. Desalination, 380 (2016) 105-111.

568 [34] J. Choi, J. Jegal, and W. Kim. Fabrication and characterization of multi-walled carbon
569 nanotubes/polymer blend membranes. J.Membr.Sci., 284 (2006) 406-415.

570 [35] Z. Spitalsky, D. Tasis, K. Papagelis, and C. Galiotis. Carbon nanotube–polymer
571 composites: Chemistry, processing, mechanical and electrical properties. Progress in Polymer
572 Science, 35 (2010) 357-401.

573 [36] V. Datsyuk, M. Kalyva, K. Papagelis, J. Parthenios, D. Tasis, A. Siokou, et al. Chemical
574 oxidation of multiwalled carbon nanotubes. Carbon, 46 (2008) 833-840.

575 [37] N.G. Sahoo, S. Rana, J.W. Cho, L. Li, and S.H. Chan. Polymer nanocomposites based on
576 functionalized carbon nanotubes. Progress in Polymer Science, 35 (2010) 837-867.

577 [38] X. Tong, B. Zhang, and Y. Chen. Fouling resistant nanocomposite cation exchange
578 membrane with enhanced power generation for reverse electrodialysis. J.Membr.Sci., 516
579 (2016) 162-171.

580 [39] P. Wang, J. Ma, F. Shi, Y. Ma, Z. Wang, and X. Zhao. Behaviors and effects of differing
581 dimensional nanomaterials in water filtration membranes through the classical phase inversion
582 process: A review. Ind Eng Chem Res, 52 (2013) 10355-10363.

583 [40] C. Fernandez-Gonzalez, A. Dominguez-Ramos, R. Ibañez, Y. Chen, and A. Irabien.
584 Valorization of desalination brines by electrodialysis with bipolar membranes using
585 nanocomposite anion exchange membranes. Desalination, 406 (2017) 16-24.

586 [41] C. Fernandez-Gonzalez, A. Dominguez-Ramos, R. Ibañez, and A. Irabien. Electrodialysis
587 with bipolar membranes for valorization of brines. Separation and Purification Reviews, 45
588 (2016) 275-287.

589 [42] J.G. Hong, Y. Chen. Nanocomposite reverse electrodialysis (RED) ion-exchange
590 membranes for salinity gradient power generation. J.Membr.Sci., 460 (2014) 139-147.

591 [43] J. Gi Hong, Y. Chen. Evaluation of electrochemical properties and reverse electrodialysis
592 performance for porous cation exchange membranes with sulfate-functionalized iron oxide.
593 J.Membr.Sci., 473 (2015) 210-217.

594 [44] S. Yang, C. Gong, R. Guan, H. Zou, and H. Dai. Sulfonated poly(phenylene oxide)
595 membranes as promising materials for new proton exchange membranes. Polym.Adv.Technol.,
596 17 (2006) 360-365.

597 [45] P.S. Goh, A.F. Ismail, and B.C. Ng. Carbon nanotubes for desalination: Performance
598 evaluation and current hurdles. Desalination, 308 (2013) 2-14.

599 [46] M. Vaselbehagh, H. Karkhanechi, S. Mulyati, R. Takagi, and H. Matsuyama. Improved
600 antifouling of anion-exchange membrane by polydopamine coating in electrodialysis process.
601 Desalination, 332 (2014) 126-133.

602 [47] H. Jaroszek, A. Lis, and P. Dydo. Transport of impurities and water during potassium
603 nitrate synthesis by electrodialysis metathesis. Separation and Purification Technology, 158
604 (2016) 87-93.

605 [48] R. Ibáñez, A. Pérez-González, P. Gómez, A.M. Urtiaga, and I. Ortiz. Acid and base
606 recovery from softened reverse osmosis (RO) brines. Experimental assessment using model
607 concentrates. Desalination, 309 (2013) 165-170.

608 [49] S. Pawlowski, P. Sistat, J.G. Crespo, and S. Velizarov. Mass transfer in reverse
609 electrodialysis: Flow entrance effects and diffusion boundary layer thickness. J.Membr.Sci., 471
610 (2014) 72-83.

611 [50] J. Yin, B. Deng. Polymer-matrix nanocomposite membranes for water treatment.
612 J.Membr.Sci., 479 (2015) 256-275.

613 [51] T. Sata, Y. Tagami, and K. Matsusaki. Transport properties of anion-exchange membranes
614 having a hydrophobic layer on their surface in electrodialysis. J Phys Chem B, 102 (1998) 8473-
615 8479.

616 [52] M. Mulder, Preparation of synthetic membranes, Basic principles of membrane
617 technology,Springer Science & Business Media (Ed.), ISBN: 9401708355, 9789401708357,
618 2013, pp. 58-59.

619 [53] P. Dlugolecki, P. Ogonowski, S.J. Metz, M. Saakes, K. Nijmeijer, and M. Wessling. On the
620 resistances of membrane, diffusion boundary layer and double layer in ion exchange membrane
621 transport. J.Membr.Sci., 349 (2010) 369-379.

622 [54] B.D. Mistry, A handbook of spectroscopic data, Chemistry (UV, IR, PMR, CNMR and
623 MAss Spectroscopy), , Oxford book company, ISBN: 987-81-89473-86-0, 2009.

624 [55] T. Sata, T. Yamaguchi, and K. Matsusaki. Effect of hydrophobicity of ion exchange groups
625 of anion exchange membranes on permselectivity between two anions. J.Phys.Chem., 99 (1995)
626 12875-12882.

627 [56] G.M. Geise, M.A. Hickner, and B.E. Logan. Ionic resistance and permselectivity tradeoffs
628 in anion exchange membranes. ACS Appl.Mater.Interfaces, 5 (2013) 10294-10301.

629 [57] M. Šíra, D. Trunec, P. Stahel, V. Buršíková, Z. Navrátil, and J. Buršík. Surface
630 modification of polyethylene and polypropylene in atmospheric pressure glow discharge.
631 J.Phys.D, 38 (2005) 621-627.

632 [58] N. Pismenskaya, N. Melnik, E. Nevakshenova, K. Nebavskaya, and V. Nikonenko.
633 Enhancing ion transfer in overlimiting electrodialysis of dilute solutions by modifying the
634 surface of heterogeneous ion-exchange membranes. Int.J.Chem.Eng., (2012).

635 [59] Y. Tanaka. Mass transport and energy consumption in ion-exchange membrane
636 electrodialysis of seawater. J.Membr.Sci., 215 (2003) 265-279.

637 [60] E. Brauns. Salinity gradient power by reverse electrodialysis: effect of model parameters
638 on electrical power output. Desalination, 237 (2009) 378-391.

639 [61] R. Takagi, M. Vaselbehagh, and H. Matsuyama. Theoretical study of the permselectivity of
640 an anion exchange membrane in electrodialysis. J.Membr.Sci., 470 (2014) 486-493.

641 [62] V.D. Grebenyuk, R.D. Chebotareva, S. Peters, and V. Linkov. Surface modification of
642 anion-exchange electrodialysis membranes to enhance anti-fouling characteristics. Desalination,
643 115 (1998) 313-329.

644 [63] M. Šupová, G.S. Martynková, and K. Barabaszová. Effect of nanofillers dispersion in
645 polymer matrices: A review. Sci.Adv.Mater., 3 (2011) 1-25.

646 [64] E.M. Vrijenhoek, S. Hong, and M. Elimelech. Influence of membrane surface properties on
647 initial rate of colloidal fouling of reverse osmosis and nanofiltration membranes. J.Membr.Sci.,
648 188 (2001) 115-128.

649